Preprints.org

Article

Not peer-reviewed version

Microtextural Characteristics of Ultramafic Rock-Forming Minerals and Their Effects on Carbon Sequestration

Tadsuda Taksavasu *, Piyanat Arin, Thanakon Khatecha, Suchanya Kojinok

Posted Date: 13 May 2024

doi: 10.20944/preprints202405.0743.v1

Keywords: carbon sequestration; climate action; enhanced rock weathering (ERW); mineralization; natural-based materials

Preprints.org is a free multidiscipline platform providing preprint service that is dedicated to making early versions of research outputs permanently available and citable. Preprints posted at Preprints.org appear in Web of Science, Crossref, Google Scholar, Scilit, Europe PMC.

Copyright: This is an open access article distributed under the Creative Commons Attribution License which permits unrestricted use, distribution, and reproduction in any medium, provided the original work is properly cited.

Preprints.org (www.preprints.org) | NOT PEER-REVIEWED | Posted: 13 May 2024 doi:10.20944/preprints202405.0743.v1

Disclaimer/Publisher's Note: The statements, opinions, and data contained in all publications are solely those of the individual author(s) and contributor(s) and not of MDPI and/or the editor(s). MDPI and/or the editor(s) disclaim responsibility for any injury to people or property resulting from any ideas, methods, instructions, or products referred to in the content.

Article

Microtextural Characteristics of Ultramafic Rock-Forming Minerals and Their Effects on Carbon Sequestration

Tadsuda Taksavasu [1,*], Piyanat Arin [2], Thanakon Khatecha [1] and Suchanya Kojinok [3]

[1] Department of Mining and Petroleum Engineering, Faculty of Engineering, Chiang Mai University; 239 Huay Kaew Road, Suthep, Muang Chiang Mai, Chiang Mai Province 50200, Thailand
[2] Department of Geological Sciences, Faculty of Sciences, Chiang Mai University; 239 Huay Kaew Road, Suthep, Muang Chiang Mai, Chiang Mai Province 50200, Thailand
[3] Institute of Product Quality and Standardization, Maejo University, Chiang Mai 50290, Thailand
* Correspondence: tadsuda.t@cmu.ac.th; Tel.: +66 81 1345 639

Abstract: Ultramafic rocks become promising candidates for carbon sequestration by enhanced carbon dioxide (CO_2) mineralization strategies due to their highly CO_2-reactive mineral composition and its abundant availability. This study reports a mineralogy and microtextures of a representative ultramafic rock from the Ma-Hin Creek in northern Thailand and observes evidence of CO_2 mineralization occurring through the interaction between CO_2 and the rock with the existence of water under ambient conditions. After sample collection, rock description was determined by optical petrographic analysis. The rock petrography reveals a cumulated wehrlite comprising over 50% olivine and minor amounts of clinopyroxene, plagioclase, and chromian spinel. Approximately 25% of the wehrlite has altered to serpentine and chlorite. A series of CO_2 batch experiments were conducted on six different rock sizes at a temperature of 40°C and pressure of 1 atm over five consecutive days. The post-experimental products were dried, weighed, and geochemically analyzed to detect changes in mineral species. Experimental results showed that product weight and the presence of calcite increased with reducing grain size. Additionally, the modal mineralogy of the wehrlite theoretically suggests a potential CO_2 uptake of up to 53%, which is higher than the average uptake values of mafic rocks. These findings support the suitable rock investigation approach and the preliminary assessment of carbon mineralization potential, contributing to enhanced rock weathering techniques for CO_2 removal that could be adopted by mining and rock supplier industries.

Keywords: carbon sequestration; climate action; enhanced rock weathering (ERW); mineralization; natural-based materials

1. Introduction

A long-term cumulative emission of carbon dioxide (CO_2) into the atmosphere has increased global atmospheric CO_2 concentration, resulting in a drastic rise of global surface temperature and a consequent climate change. In 2018, the Intergovernmental Panel on Climate Change (IPCC) suggested several climate actions that aim to limit the global temperature increase responding to the Paris Agreement [1,2]. One of the promising strategies for contributions to CO_2 emission reduction and atmospheric CO_2 removal has been known as carbon capture and storage (CCS) technology [3–5]. CCS is an integrated technology comprising (i) CO_2 capturing whether from an emitting source or atmosphere combined with a CO_2 separating procedure, (ii) source-to-sink transportation, and (iii) CO_2 storing permanently and effectively. The most suitable options for CO_2 storage include sequestration in subsurface geological formations, and carbon mineralization [4,6–8].

Carbon mineralization, hereby called the CO_2 mineralization, requires an occurrence of mineral formations rich in divalent cations, including Mg^{2+}, Ca^{2+}, and Fe^{2+}, to combine with molecules of CO_2, resulting in a permanent lock away of CO_2 in the forms of stable solid carbonate minerals. CO_2 mineralization is a safe CCS technique rising in many countries, especially where underground CO_2 injecting and storing activities are not applicable [9,10]. Mineralized carbonate products and

© 2024 by the author(s). Distributed under a Creative Commons CC BY license.

Preprints.org (www.preprints.org) | NOT PEER-REVIEWED | Posted: 13 May 2024 doi:10.20944/preprints202405.0743.v1

noncrystalline silica byproducts can be attributed to a variety of utilizations in many industries [11–13]. The most common CO_2-reactive minerals are formed in magnesium-, calcium-, or iron-bearing silicate groups such as olivine, serpentine, pyroxene, amphibole, and plagioclase. Each mineral has a different capacity of CO_2 uptake potential, ranging from 63 to 16%, depending on the thermodynamic properties and elemental availability [11,14–19]. Uncertainty in the mineral assemblage of real-world rock formations affects diverse values of CO_2 uptake estimation.

CO_2 mineralization of the promising minerals is spontaneous and exothermal and naturally occurs as rock chemical weathering and subsequent atmospheric CO_2 removal [20–23], but it has slow reaction rates. Over decades, numerous experimental methods and conditions accelerating the CO_2 mineralization of mineral or rock targets have been proposed (e.g., [24–32]). The methods include element extraction, mineral processing, and specific treatments using heat, pressure, and chemicals, which unsurprisingly require lots of energy consumption, infrastructure, and costs. It is also worth exploring another alternative option for carbon removal. Enhanced rock weathering (ERW) is one of the attractive engineered practices to speed up the natural CO_2 removal from the air [2,7,19,33–36]. The technique involves increasing surface areas of CO_2-reactive rocks by finely grinding methods and then applying the rock powder over lands, coasts, or in the oceans [8,35,37–39]. Selecting suitable rock types for ERW is very important in maximizing the reaction rates and ultimately offering the greatest CO_2 uptake capacity [10,36,40,41]. In addition to rock types, the abundance of rock resources essentially yields unlimited capacity for CO_2 sequestration.

Ultramafic igneous rocks and their metamorphosed versions play an important role in the global supply of favorable CO_2 reactive minerals, consisting of over 90% olivine, pyroxene, and amphibole with minor amounts of plagioclase and trace quantities of other minerals. The ultramafic rocks form through the crystallization of deep magmas rich in Mg, Ca, and Fe silicates, occurring from the middle-to-lower crusts to the upper mantle of the Earth. The rock formations are normally uplifted to near-surface conditions or exposed to the surfaces driven by tectonic events resulting in gigantic massifs of ophiolites or various scaled layered intrusions, which later undergo natural hydration of the anhydrous silicate minerals and subsequent carbon mineralization at varied rates [42–46]. The mineralization of CO_2 in ultramafic rocks occurs when the formations interface with CO_2 in the air or CO_2-dissolved groundwaters flowing through rock fractures. These result in the formation of carbonate minerals, especially calcite or magnesite, coexisting with quartz or noncrystalline silica formed as open-space filling veins. According to relatively high CO_2 reactivity and global availability of ultramafic rock resources, these rocks are potentially considered the most promising materials for the development of ERW methods supporting atmospheric carbon dioxide removal technology.

Based on mineralogical variations, ultramafic rocks are divided into several groups, such as dunites, peridotites, pyroxenites, amphibolites, and serpentinites, which can also be subdivided into numerous types. Each type provides a specific amount of promising minerals that affects variable CO_2 uptake potential [31,40,47–49]. Besides the mineralogy, their microtextural characteristics, including mineral grain size, and alteration level, additionally influence the CO_2 mineralization potential that can be applied to the ERW strategies. To closely assess the CO_2 mineralization potential of any rock, it is necessary to deeply understand the rock mineralogy in terms of mineral types, quantities, textures, and alteration degrees.

This study focuses on a primary mineralogical assessment of real-world ultramafic rock exposure in Thailand, SE Asia, for CO_2 uptake potential based on a modal composition and batch experiments. In this research, the potential occurrence of CO_2 mineralization has been observed through the experimental works between the selected ultramafic sample and CO_2-bearing water. The experiments are investigated at different particle sizes, and all are conducted under ambient conditions resembling the natural rock weathering process. The primary evidence for the existing CO_2 mineralization is observed and described as the changes in the mineralogical composition and weight of the obtained products compared to the initial rock. This study additionally attempts to provide a fundamental strategy to determine and evaluate suitable rocks supporting ERW techniques that could be applied in further mining and rock supplier industries elsewhere.

2. Geological Background

Preprints.org (www.preprints.org) | NOT PEER-REVIEWED | Posted: 13 May 2024 doi:10.20944/preprints202405.0743.v1

The study area is located in Phrao District of Chiang Mai Province, Northern Thailand. The rock formation in this area comprises three units as shown in Figure 1. From lower to upper formations, there are Middle-Upper Carboniferous sedimentary rocks, Permian basaltic-to-andesitic volcanic rocks, and Permian limestones, which are mostly formed in subaqueous environments [50]. These units are slightly metamorphosed and altered. The outcrops and floated rocks of cumulus ultramafic rocks, such as dunite and peridotite, were also discovered along the Ma-Hin Creek and its distributary channels in the volcanic terrain [51]. These units have been interpreted as part of the Chiang Rai-Chiang Mai Volcanic Belt formed in back-arc and oceanic basin environments and potentially represented relics of the Palaeo-Tethys Ocean, which separated the Shan-Thai and Indochina cratons [52,53]. The emergence of ultramafic rocks in the study area is a result of a closure of the Palaeo-Tethys Ocean in the Late Triassic induced by an oceanic crust subduction and a subsequent collision of the cratons forming a suture zone. These particular tectonic events mainly influence numerous reverse and thrust faults allowing deep-seated plutons or intrusions to be uplifted and exposure to surfaces or near-surface environments.

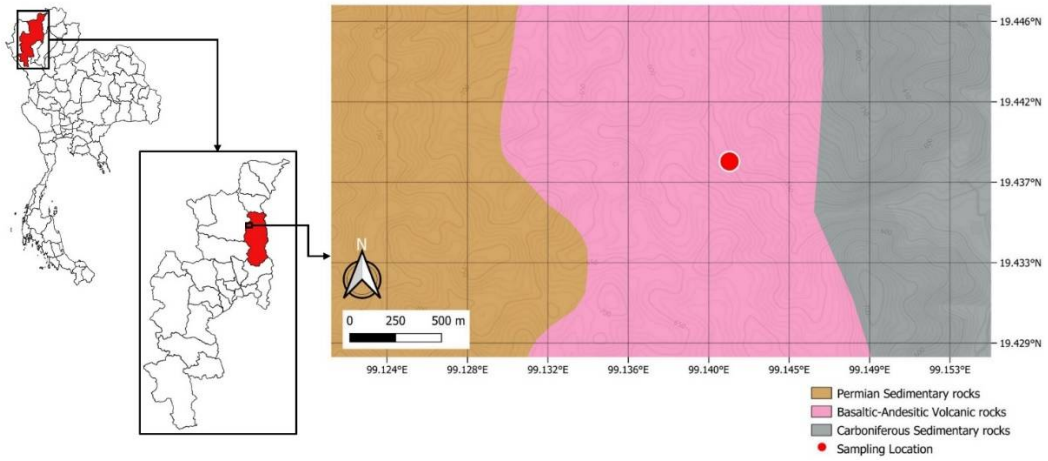

Figure 1. Geologic map of the study area located in Phrao, Chiang Mai, Northern Thailand, showing three rock units at a scale of 1:50,000 modified from the Thailand Department of Mineral Resources (DMR) [54]. The location of sampling is in the volcanic terrain indicated by a red dot. The contour interval is 20 meters.

3. Materials and Methods

3.1. Rock Sampling and Petrographic Analysis

The rock floats were collected in the Ma-Hin Creek, located in Phrao district, Chiang Mai, northern Thailand. The rock specimens are massive and dense exhibiting dark green to black fresh colors. The tarnished colors are found to be yellowish-to-reddish brown and dark brown. The specimens show coarse-sized crystalline textures of intrusive igneous origins as presented in Figure 2. The standard petrographic thin sections were prepared with the equipment from the thin-section commercial lab. The finished product is a polished slice of 30-micron-thick rock specimen mounted onto a 27×46 mm t glass slide glued with a covered glass. Two thin sections were observed under the transmitted light of a conventional petrographic microscope at the Department of Geological Sciences, Chiang Mai University, to obtain data including modal mineral composition, microtextural characteristics, and alteration features. The modal mineralogy was determined by 400 point counting per thin section and was normalized to 100%. The rock description here is based on the standard of the International Union of Geological Sciences, known as IUGS [55].

Preprints.org (www.preprints.org) | NOT PEER-REVIEWED | Posted: 13 May 2024 doi:10.20944/preprints202405.0743.v1

Figure 2. Rock samples collected from the study area at the Ma-Hin Creek, Phrao District of Chiang Mai exhibiting dense greenish grey-to-black coarse crystalline textures.

3.2. Experimental Procedure

Batch experiments between the rock sample and CO_2-bearing water were performed in an ambient condition resembling as close as possible the rock weathering process. The methods were conducted in the lab at the Department of Mining and Petroleum Engineering, Chiang Mai University.

Prior to batch experiments, the sample undergoes a mechanical pre-treatment method to increase its possible reactive surface area for the interaction which states as follows. First, the rock specimens were cut and grinded into small pieces using the jaw crusher and the grinding machine. Then, the ground sample was separated into six groups based on their particle sizes through a dry-sieving analysis. These include the U.S. mesh sizes of 18, 35, 60, 120, 230, and pan. The top three coarsest particle sets were individually weighed for 10 grams, whereas the remaining sets were weighed for 5 grams.

Each sample was put into a 600 ml beaker filled with 250 ml of deionized water producing a slurry. The CO_2 in a gaseous phase was then introduced to the slurry through a 3 mm rubber hose under ambient pressure conditions with a constant rate of CO_2 bubbling. Lastly, a glass-coated magnetic stirring bar was added. The beaker was partially sealed by aluminum foil and placed on a hotplate magnetic stirrer. The mixture was stirred at a speed of approximately 1,000 rpm and a temperature of 40°C for 60 hours. The flow diagram is presented in Figure 3. Thereafter, the stirring bar and the CO_2 hose were carefully removed from the retrieved mixture. The beaker containing the mixture product was subsequently placed in an oven set at 60°C until it completely dried. The weights of the final products were measured to determine a relationship between weight change and particle size.

Preprints.org (www.preprints.org) | NOT PEER-REVIEWED | Posted: 13 May 2024 doi:10.20944/preprints202405.0743.v1

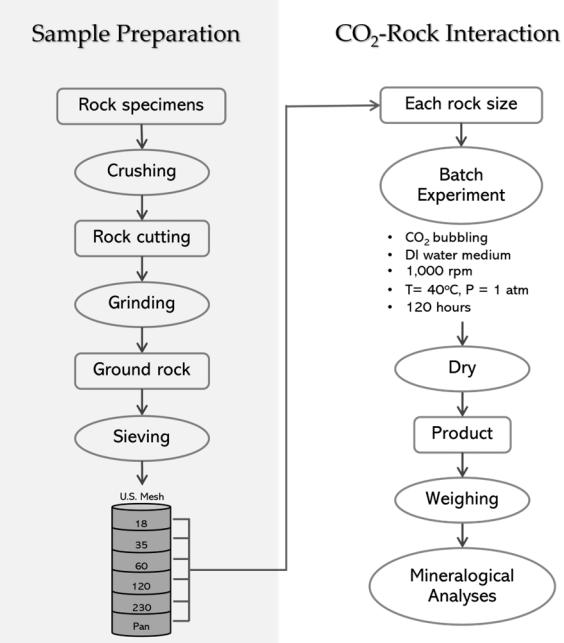

Figure 3. Flow diagram of CO_2-rock batch experiments and a preparation method conducted in this study. The preparation method includes increasing surface areas by crushing and grinding of the rock samples and separating the ground rocks into six mesh sizes by a sieving process.

3.3. Mineralogical Analysis

The post-experiment products were analyzed mineralogically and geochemically. X-ray diffraction analysis (XRD) was conducted at the Department of Geological Sciences, Chiang Mai University, to characterize the mineralogy and crystal structures of the initial rock sample and its products. The obtained products were powdered and analyzed using a BrukerD8Advance diffractometer equipped with a copper anode. An x-ray wavelength of 1.540598 Å and an accelerating voltage of 40 kV were used, with a filament current of 30 mA. Step scan XRD data was collected over a range of 2°–70°2θ with a step width of 0.04°2θ and a counting time of 1 second per step. Mineral identification and quantification of the products were performed using the EVA software and referencing the patterns from the International Centre for Diffraction Data (ICDD) database. The availability of mineral components and the XRD patterns of these materials were then compared.

The selected products were imaged using the TESCAN CLARA Schottky field emission scanning electron microscope (FE-SEM) at the Institute of Product Quality and Standardization, Maejo University. The materials were individually mounted on aluminum stubs and gold coated. The images were taken in secondary electron mode with a working distance of 8.19–9.90 mm and an acceleration voltage of 15.0 kV. The elemental compositions of these materials were obtained and analyzed by the Oxford Ultim Max energy-dispersive X-ray spectrometer (EDS), which is coupled with the FE-SEM and the Aztec software.

4. Results

4.1. Mineral Composition and Microtextural Characteristics

Under a microscopic view, the sample exhibits a cumulate texture comprising coarse-grained cumulus crystals of olivine and chromium spinel surrounded by fine-grained intercumulus crystals of pyroxene and plagioclase (Figure 4). Based on the modal mineralogical investigation, the sample has 74.5% primary minerals consisting of approximately 56.75 model% olivine, 9.25% clinopyroxene, 6.5% plagioclase, and 2% chromian spinel. The secondary minerals, on the other hand, are results from the alteration of the primary minerals. They comprise 25.5 modal% serpentine and chlorite exist in the relict shapes of the primary minerals. Trace amounts of clay minerals are barely observed. Detailed mineralogy and microtextures of each mineral are provided below.

Preprints.org (www.preprints.org) | NOT PEER-REVIEWED | Posted: 13 May 2024 doi:10.20944/preprints202405.0743.v1

Olivine is the most abundant mineral forming euhedral elongate-to-equant crystals with irregular fractures. Its average size ranges from 0.1 to 2.5 mm. Approximately 30–70% of the olivine is altered to serpentine and chlorite. The remnant olivine shapes are still preserved.

The second most abundant mineral is pyroxene, which forms anhedral intercrystals having 0.1–0.7 mm in size. The pyroxene distinctly exhibits inclined extinction that refers to clinopyroxene members such as diopside, hedenbergite, pigeonite, and augite. The alteration of clinopyroxene to become chlorite and brownish amphibole occurs at 10–30%.

The plagioclase exhibits anhedral crystals with multiple twinning. It has a size ranging from 0.1 to 0.5 mm. The minerals are highly altered to clay minerals and fine-grained micas known as sericite. The chromian spinel exhibiting euhedral opaque crystals has a diameter ranging from 0.1–0.7 mm with less than 30% degree of alteration.

According to the standard IUGS ultramafic rock classification, this study considers the ternary diagram with olivine, orthopyroxene, and clinopyroxene, known as the Ol–Opx–Cpx ternary plot. The recalculated modal proportion of the primary mineralogy of this rock falls into the zone of wehrlite as the rock contains 85.98% olivine and 14.02% clinopyroxene with the absence of orthopyroxene as shown in Figure 5.

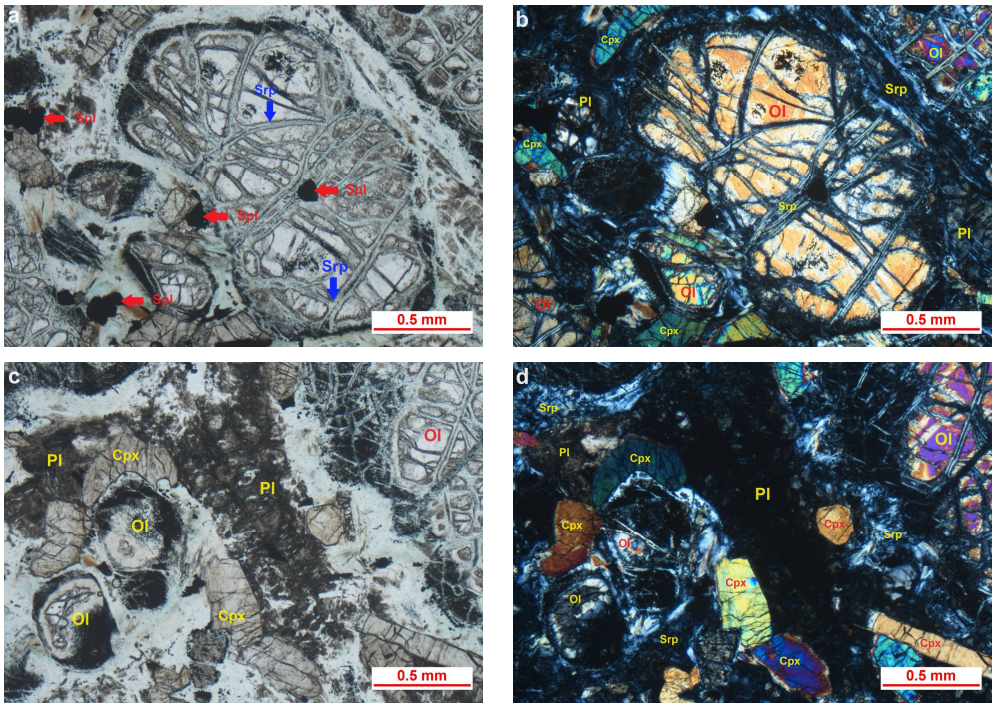

Figure 4. Photomicrographs of the wehrlite exhibiting a cumulate texture that comprises primary and secondary minerals. (**a**) Opaque spinel crystals and pale green colored serpentine are observed under plane-polarized light indicated by the red and blue arrows, respectively. (**b**) Corresponding crossed-polarized light image showing serpentine-filling fractured olivines associated with finer crystals of clinopyroxene and plagioclase. (**c**) Plagioclase and some olivine grains are being altered observed under plane-polarized light. Their original morphologies are preserved. (**d**) Corresponding crossed-polarized light image showing the alteration products of plagioclase and olivine are clay minerals and serpentine, respectively. Abbreviation: Cpx=clinopyroxene, Ol=olivine, Pl=plagioclase, Spl=spinel, Srp=serpentine.

Preprints.org (www.preprints.org) | NOT PEER-REVIEWED | Posted: 13 May 2024 doi:10.20944/preprints202405.0743.v1

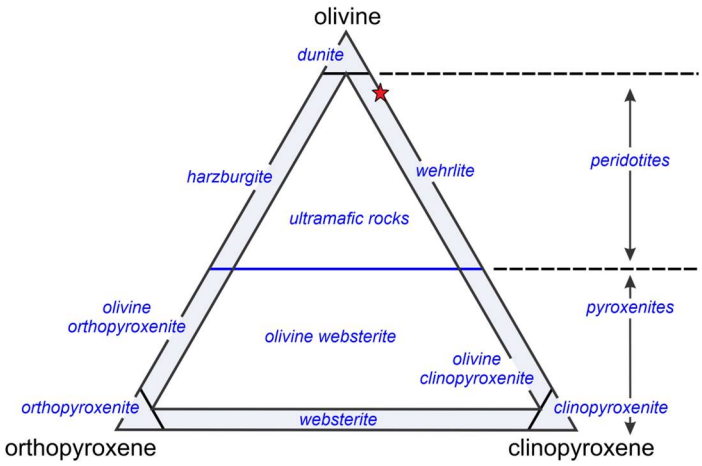

Figure 5. The standard IUGS classification ternary diagram for ultramafic rocks based on a proportion of olivine, orthopyroxene, and clinopyroxene, also called the Ol–Opx–Cpx diagram. The studied rock sample falls on a zone of wehrlite represented by a red star symbol.

4.2. Weight Changes

The batch experiments of the wehrlite samples in all particle sizes have resulted in their increasing weights, as recorded in Table 1. The finest sample has experienced the highest percentage of weight gain, whereas the coarsest sample has shown the opposite. Possible factors influencing the sample weight gain are discussed in the following sections.

Table 1. Weight comparisons of the wehrlite samples in various sizes measured between pre-test and post-test conditions.

Sample ID	Mesh No.	Particle Size (mm)	Weight (g)		Difference (g)	% Change
			Pre-test	Post-test		
PR-18	18	≥ 1.0	10.000	10.004	+ 0.004	0.04
PR-35	35	< 1.0 – 0.5	10.000	10.006	+ 0.006	0.06
PR-60	60	< 0.5 – 0.25	10.000	10.010	+ 0.010	0.10
PR-120	120	< 0.25 – 0.125	5.000	5.016	+ 0.016	0.32
PR-230	230	< 0.125 – 0.0625	5.000	5.015	+ 0.015	0.30
PR-silt	Pan	< 0.0625	5.000	5.018	+ 0.018	0.36

4.3. Mineralogical Changes

The powder X-ray diffraction data of the original wehrlite sample and its post-experiment products show discrete peak patterns as presented in Figure 6. The XRD pattern of each sample is influenced by all mineral phases formed in that sample. The minerals forming well-defined crystalline structures certainly result in narrow and sharp peaks, whereas the noncrystalline or amorphous phases induce a peak broadening. The diffraction pattern is thus a combination of the diffraction pattern of each phase. However, the heterogeneity in the mixture composition, especially the whole-rock sample provided by this study, certainly affects complicated diffraction patterns.

The compositional variations including mafic minerals (olivine, augite, albite, antigorite), clay minerals (chlorite, illite), and carbonates (calcite), are presented in Table 2. Antigorite, an indicative of serpentine-group minerals, is a major mineral (35.62%) of the initial rock, however, this mineral becomes a minor phase (8.83%) in the 35-mesh-sized product. Olivine and augite are found as moderate minerals (22.14% and 25.33%, respectively) in the initial wehrlite and become minor phases

Preprints.org (www.preprints.org) | NOT PEER-REVIEWED | Posted: 13 May 2024 doi:10.20944/preprints202405.0743.v1

(3.99–7.28%) in the products exhibiting mesh sizes of 60 and 120. On the other hand, calcite is originally observed as a minor phase (9.95%) and turns to a moderate phase (10.84–19.18%) in the 35-mesh, 60-mesh, 230-mesh, and below 230-mesh-sized products. Magnesium-bearing calcite is detected as a minor phase (3.56%) only in the 18 mesh-sized product, whereas calcium-bearing albite is only found in the 60-mesh-sized product as a moderate phase (21.08%).

The products in 120-mesh-sized and silt-sized particles have been selected for FE-SEM imaging and EDS analysis due to their significant amounts of calcite, surface area, and weight gain. The FE-SEM images indicate two different surface morphologies including irregular surfaces and smooth surfaces. The EDS spectra of the two features show discrete elemental compositions. In Figure 7, the irregular surfaces, which are locally observed in the 120-mesh-sized product, are in the form of encrusting materials. The surfaces display the main contributions of oxygen, carbon, and magnesium, which may be expected for new magnesium-bearing carbonate species. The EDS spectrum of the smooth surface, on the other hand, shows magnesium, silicon, and oxygen signals of the nonreacted rock-forming silicate minerals. In Figure 8, an aggregate of very fine-grained polycrystalline solid materials is observed on the silt-sized product forming irregular surfaces. This aggregate exhibits a strong calcium and oxygen signal on the EDS spectrum, which is expected for calcite. Its smooth surface unsurprisingly displays a strong magnesium, silicon, and oxygen signal that may be considered as nonreacted silicate minerals of the wehrlite.

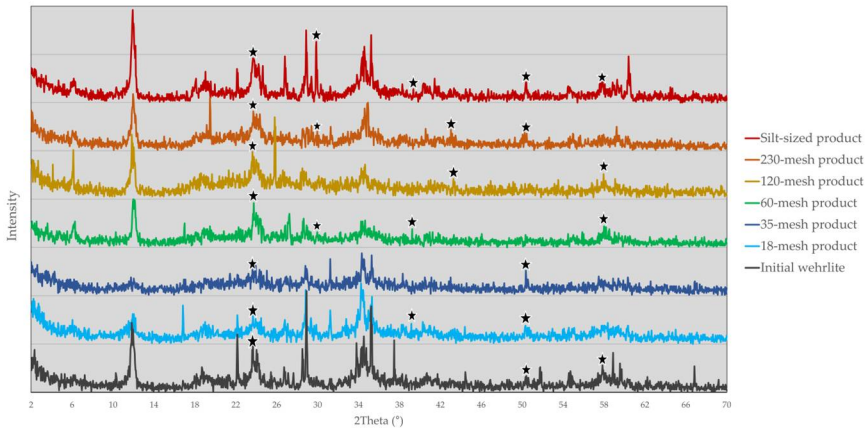

Figure 6. X-ray diffractograms of the wehrlite and its post-experiment products exhibiting discrete peak patterns that were possibly induced by the transformations of the primary mineral assemblage during CO_2-rock interactions. The calcite XRD peaks are indicated by black star symbols.

Table 2. X-ray diffraction analysis of the initial wehrlite and its products obtained from the batch experiments.

Sample Material	**Major phase** [>30%]	**Moderate phase** [10-30%]	**Minor phase** [2-10%]	**Trace phase** [<2%]
Wehrlite	Antigorite	Augite Olivine	Calcite Albite Chlorite	Illite
18-mesh product	n/d	Antigorite Augite Olivine Albite	Chlorite Mg-bearing calcite	Illite
35-mesh product	Olivine	Albite	Antigorite	Chlorite

Preprints.org (www.preprints.org) | NOT PEER-REVIEWED | Posted: 13 May 2024 doi:10.20944/preprints202405.0743.v1

Sample Material	**Major phase** [>30%]	**Moderate phase** [10-30%]	**Minor phase** [2-10%]	**Trace phase** [<2%]
		Calcite Augite		Illite
60-mesh product	Antigorite	Ca-bearing albite Calcite	Chlorite Illite Olivine	Augite
120-mesh product	Albite	Antigorite Illite	Calcite Olivine Augite Cr-bearing chlorite	n/d
230-mesh product	n/d	Antigorite Olivine Augite Illite Calcite	Chlorite Albite	n/d
Silt-sized product	Antigorite	Augite Calcite Albite Olivine	Chlorite	Illite

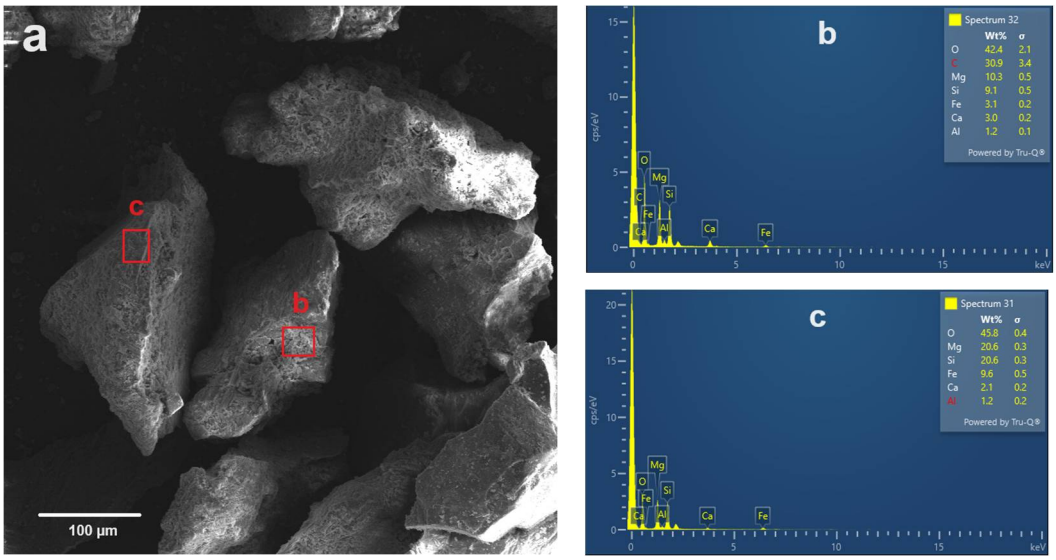

Figure 7. FE-SEM image and area-selected EDS spectra of the 120-mesh-sized product resulted from batch experiment: (**a**) The product overall exhibits individual massive grains. Those grains show likely smooth surface associated with irregular rough encrusted materials. (**b**) The EDS spectrum of the irregular encrusting materials mostly shows high C and O concentrations with a significant Mg signal. (**c**) The EDS spectrum obtained from the smooth surface, on the other hand, shows high Mg, Si, and O signal.

Preprints.org (www.preprints.org) | NOT PEER-REVIEWED | Posted: 13 May 2024 doi:10.20944/preprints202405.0743.v1

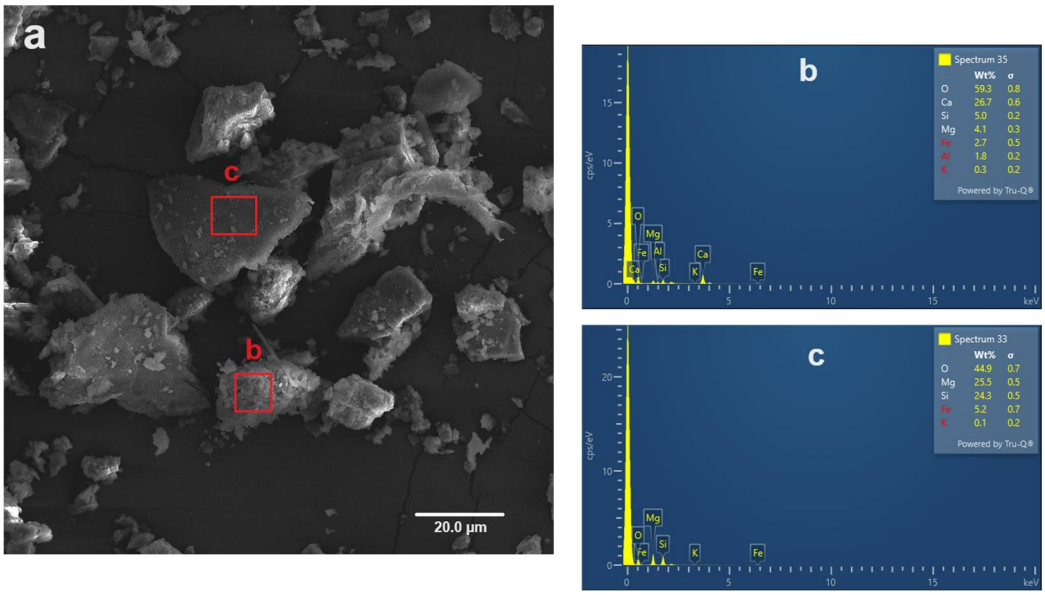

Figure 8. FE-SEM image and area-selected EDS spectra of the silt-sized product resulted from batch experiment: (**a**) The product overall exhibits individual silt-sized grains having smooth dense surface. Very fine-grained solids showing sizes of <2 µm in diameter are observed accumulating on the product surface. (**b**) The EDS spectrum of the accumulated grains shows high Ca and O concentration. (**c**) The EDS spectrum obtained from the smooth surface shows the opposite as it exhibits high Mg, Si, and O signal.

5. Discussions

5.1. Evidence for the Occurrence of Carbon Mineralization

The existence of the interactions between CO_2 and rock at any degree essentially affects the transformation of the properties of that particular rock, such as its mineral assemblages, density or weight, and microtextural characteristics. These physiochemical changes can be detected on any scale provided in the following details.

The increasing weight of all-sized products after the batch experiments corresponds to the increase in density resulting from mineral abundance. Each mineral has a particular range of density calculated from its weight and volume. Changes in the rock-forming mineral composition subsequently cause the initial density of the rock to change. A previous study by Cutts et al. (2021) constrained the relationships and changes in physical and chemical properties during the serpentinization and carbonation of the ophiolitic ultramafic rocks. They suggested that this coupling process results in systematic fluctuating densities induced by the current mineral assemblages formed in the rocks. This potentially supports one of the findings of this study, as the product weight changes reflect the changes in its mineralogy. Thus, the weight gains of products obtained from this study provide primary evidence of mineralogical changes affected by enhanced weathering interactions. Small degrees of weight changes, which are less than 1%, might be effects of slow reaction rates and reaction efficiency. However, it should be noted that determining only the sample weight change alone is not likely sufficient.

The discrete XRD peak patterns and peak heights among the before- and after-experiment samples indicate their mineralogical and crystallographic variations. Compared to the initial wehrlite, the mineral phases of all-sized products have been changed in various degrees and directions, which are consequences of the reaction with CO_2-bearing waters. Most previous analytical experiments account for the presence of magnesite and noncrystalline silica as a final result of carbon mineralization [12–14,26]. In this study, there is an absence of pure magnesite. Calcite, on the other

Preprints.org (www.preprints.org) | NOT PEER-REVIEWED | Posted: 13 May 2024 doi:10.20944/preprints202405.0743.v1

hand, is mostly found as a dominant carbonate mineral precipitated in all products. Magnesium-bearing calcite and calcium-bearing plagioclase are locally detected in coarse-to-medium-grained products. The lack of magnesite and silica formation in this study can be explained by a short availability of magnesium cations in the aqueous solution, which is possibly limited by experiment conditions (temperature, pressure), chemistry of the medium (pH, salinity, ion activity), purity of rock (amount of ion supply), and time (for dissolution, for precipitation). Increasing amounts of calcite phases detected in the products are adequate for the carbonate formation as a result of CO_2 mineralization. This study agrees that differences in diffraction patterns between the initial rock and its CO_2 batch products have pointed to the changes in crystallographic structures and mineral assemblages resulting from the existing CO_2-rock interaction. This data is necessary to provide another mineral evidence for the occurrence of CO_2 mineralization through the rock weathering process.

In addition, imaging with FESEM-coupled EDS analysis of the selected products reveals morphological evidence of calcite precipitation during the CO_2-rock interaction. The irregular plates encrusted on the original smooth surfaces of the samples are formed by the reactions between dissolved CO_2 and target CO_2 reactive rock-forming minerals. The reactions result in the aggregates of tiny grains of new mineral phases occurring along the interfaces between the rock and aqueous solution. The presence of carbon signals on the EDS spectra of the irregular crusts in combination with oxygen and calcium signals could potentially be indicative of the formation of carbonates.

5.2. Grain-Size Effects

The physiochemical changes of the products somehow vary with the particle sizes. The microtextural characteristics of the studied wehrlite confirm that the olivine crystals range from 0.1 to 2.5 mm in diameter, whereas other minerals have average crystal sizes of 0.1-0.5 mm. As larger reactive surface areas tend to be more favorable for the interaction process, decreasing the sample size by crushing it into pieces and grinding it into fine powder effectively increases the magnitude of the sample surface area. This method potentially breaks down and extracts individual target minerals, such as olivine and pyroxene, from the rocks allowing the increase of CO_2-reactive interfaces. For example, reducing the size of olivine from 2.5 mm to 0.25 mm subsequently produces 10 times more surface area in the remaining volume.

The increasing weight of the finest product exhibiting less than 0.0625 mm in diameter probably refers to the relatively high interaction rate, which was influenced by the largest surface area. The identical results are significantly observed on the products having sizes of 0.0625-0.25 mm. Based on the weight observation, these findings certainly agree with the relationships of grain sizes and interacting surface areas. According to the X-ray diffraction patterns, significant increases in calcite counting rates are found in the products having sizes of 0.25-1.0 mm and <0.0625-0.125 mm. These are equal to the average sizes of the reactive olivine, pyroxene, and other minerals formed in the rock. Lacks calcites are detected in the coarser grains due to their smaller surface areas. The results of this study confirm that the occurrence of CO_2-rock interaction of ultramafic rocks is driven by the particle sizes besides their mineralogy.

In general, the average grain size of a single mineral differs in different rock types, especially igneous rocks [56]. The rocks formed by rapid crystallization of magmas at shallow depths produce finer textures compared to those formed by steady crystallization in deep-seat magmatic chambers, which produce relatively coarse-grained textures. According to the thin-section observation, different minerals in the same rock formation widely differ in average grain size, shape, and area. This feature has been interpreted as a result of the sequence of magmatic crystallization and reaction series, which a rock had formed. The microtextural characteristics of the wehrlite studied here visibly indicate the specific magmatic sequence as it is formed by a first crystallization of coarse-grained chromian spinel, then a following olivine crystallization, and a formation of relatively fine-grained plagioclase, clinopyroxene, and Fe-Ti oxides at a final stage. The microtextural investigation provides an idea for the optimal grain-size selection of any potential rocks for ERW. Understanding the detailed mineralogy and rock characteristics highly assists in either the development of engineering designs

Preprints.org (www.preprints.org) | NOT PEER-REVIEWED | Posted: 13 May 2024 doi:10.20944/preprints202405.0743.v1

for future carbon mineralizing plants or the improvement in the mining process and production of the rock supplier industries.

5.3. Rock Mineralogy versus CO_2 Uptake Prediction

CO_2 uptake generally refers to an amount of CO_2 equivalent that can potentially be absorbed by a mineral or material through carbon mineralization. It can be determined by several approaches whether from a direct measurement of the CO_2 content of the minerals obtained from laboratory chemical reactions or a theoretical calculation based on an ideal mineral reactivity with CO_2 [57–59]. Prediction of potential CO_2 uptake of the wehrlite in this study accounts for the sum of mineral reactivity with CO_2 in the presence of water retrieved by previous literature [11,14,15,18]. The minerals used in the calculation of this study include olivine, pyroxene, serpentine, and plagioclase. The subsequent numerical product refers to a potential amount of CO_2 uptake by that rock when the reactions for carbon mineralization have been fully completed. CO_2 uptake generally shows in a unit of a percent weight by weight.

As each mineral varies in chemical composition, they show different abilities of potential CO_2 uptake. Mg-rich olivine has the highest uptake potential, which is approximately 62.5%, while pyroxene, in the form of augite, shows 37%. This means a smaller amount of olivine is required to store a ton of CO_2 compared to pyroxene. In other words, to sequester a ton of CO_2, we must have 1.6 tons of olivine or 2.7 tons of augite. Serpentine, in the form of antigorite, has 47.6% uptake potential, which requires 2.1 tons for a ton of CO_2 stored. Plagioclase exhibits less amount of potential CO_2 uptake as it shows only 16%. The mineralized products are formed as carbonates with relevant amounts of the feed minerals.

Mineralogical variation and mineral content of rocks certainly affect the difference in total CO_2 uptake estimation. The most abundant mineral formed in the rock appears to yield an ability of CO_2 uptake for the whole rock. Based on the modal mineral content obtained by petrographic analysis, the wehrlite has a potential CO_2 uptake of 52.07%, accounting for the completion of carbon mineralization of the four reactive minerals mentioned earlier. This calculated number explains that every ton of CO_2 sequestered requires 1.9 tons of the wehrlite. However, the wehrlite mineralogy obtained from XRD analysis confirms that half the amount of the olivine phase has been altered to pyroxene, serpentine, and chlorite. A decreasing amount of olivine and increasing amounts of serpentine and pyroxene cause a reduction in the uptake potential, as it shows 41.95%. To store a ton of CO_2, around 2.4 tons of the altered wehrlite are required. The required quantities of the ultramafic wehrlite for CO_2 sequestration are much lower than the average value of mafic rocks, especially basalts. Approximately 5 tons of basalts are required to trap one ton of CO_2 [17,18,60]. It is suggested that the wehrlite has the potential for CO_2 uptake by mineral traps and becomes a suitable rock for further development in the enhanced weathering approach.

Besides the CO_2 uptake potential, the availability of rock resources significantly provides the sufficiency of reactive minerals. For instance, sequestering a 100 Mt CO_2 by carbon mineralization through the ERW technology requires 190–240 Mt of the wehrlite. Exploration of the ultramafic rock deposits and geological surveys are important to further augment the precision of resource estimation for providing a sufficient amount of a mineral target.

This study strongly supports that it is crucial to conduct a primary assessment of the CO_2 uptake potential of the rocks based on their mineral contents at any scale. The mentioned analytical techniques are straightforward and help in making a basic decision for suitable rock selection. Furthermore, it should be noted that more advanced methods for quantifying the carbon uptake of other minerals and a better understanding of their reaction kinetics, efficiencies, and behaviors, are strongly recommended.

6. Conclusions

The batch experiments involving CO_2-dissolved water and various-sized ultramafic wehrlite that are performed under ambient conditions resembling natural rock weathering processes, potentially reveal several evidence for the occurrence of CO_2-rock interaction with the presence of

Preprints.org (www.preprints.org) | NOT PEER-REVIEWED | Posted: 13 May 2024 doi:10.20944/preprints202405.0743.v1

water. Firstly, the increasing weight of all products indicates an increase in density of the initial rock caused by changes in mineral assemblage and possibly the molecular weight of CO_2 turning into solid phases. Secondly, the mineralogical changes observed in the products analyzed by the X-ray diffraction patterns serve as major evidence of the reaction of rock-forming minerals with CO_2. However, this analytical method is used solely to provide comparative geochemical data on all products to better understand the relationships between grain sizes and the relative degrees of interaction. Lastly, the existence of calcite formation is key in providing further proof of emerging carbon mineralization. Calcites form as crustal layers exhibiting irregular surfaces along the interfaces between rock particles and solutions. The amount of calcite and weight gain vary in different grain sizes of the products due to the difference in surface areas. The most reactive sizes proposed by this work consistently align with the average sizes of olivine or other CO_2-reactive minerals formed in the rock. This study positively supports that optimal grain sizes used for ERW should be relevant to the average size of the most CO_2-reactive minerals abundant in the rocks.

Estimating the potential CO_2 uptake through theoretical calculation based on mineralogical observation offers new insights into the basic evaluation of suitable rocks for carbon sequestration. The wehrlite of this study, for example, shows a CO_2 uptake range from 41.95% to 52.57%. A higher uptake value likely indicates the fresh rock condition, whereas a lower uptake value stands for the altered version of the rock. Although most ultramafic rocks seem to be promising candidates for carbon sequestration by CO_2 mineralization, a comprehension of their mineralogy and microtextural characteristics is necessary to advance estimated CO_2 uptake potential leading to suitable rock selection. Leading to the future development of enhanced weathering strategies for this rock type, more advanced analytical methods in broader condition regimes associated with an assessment of resource availability have been highly recommended.

Supplementary Materials: The following supporting information can be downloaded at the website of this paper posted on Preprints.org, PetrographicAnalysis.docx containing details of petrographic study that includes Table S1 and Figures S1-S7; PowDLLXRD.xlsx containing converted raw data of all materials; individual EMF files of XRD results; individual petrographic images of the studied sample.

Author Contributions: Conceptualization, T.T.; methodology, T.T. and T.K.; validation, T.T. and S.K.; formal analysis, T.T. and P.A.; investigation, T.T., P.A., T.K. and S.K.; resources, T.T., P.A., and S.K.; data curation, T.T. and S.K.; writing—original draft preparation, T.T.; writing—review and editing, P.A., T.K. and S.K.; visualization, T.T.; supervision, S.K.; project administration, T.T.; funding acquisition, T.T. All authors have read and agreed to the published version of the manuscript.

Funding: This research was funded by CMU Junior Research Fellowship Program, grant number JRCMU2566R_051.

Data Availability Statement: The original contributions presented in the study are included in the article and supplementary materials, further inquiries can be directed to the corresponding author.

Acknowledgments: The authors thank the San-Sai Subdistrict Administrative Organization and the Office of Nong-Pid Village for their assistance throughout the fieldworks and for permission to collect and use the samples. The authors sincerely thank Asst. Prof. Dr. Suparit Tangparitkul, Department of Mining and Petroleum Engineering, Chiang Mai University, for his support and guidance on laboratory work.

Conflicts of Interest: The authors declare no conflicts of interest.

References

1. UNFCCC. Paris Agreement. **2015**.
2. IPCC. *IPCC special report on Global Warming of 1.5 ◦C*; 2018.
3. Chalmers, H.; Gibbins, J. Carbon capture and storage: The ten year challenge. *Proc. Inst. Mech. Eng. C: J. Mech. Eng. Sci.* **2016**, *224*, 505-518, doi:10.1243/09544062jmes1516.
4. NASEM. Carbon Mineralization of CO2. In *Negative emissions technologies and reliable sequestration: a research agenda*; The National Academies Press: Washington, DC, 2019.
5. Wang, P.-T.; Wei, Y.-M.; Yang, B.; Li, J.-Q.; Kang, J.-N.; Liu, L.-C.; Yu, B.-Y.; Hou, Y.-B.; Zhang, X. Carbon capture and storage in China's power sector: Optimal planning under the 2°C constraint. *Appl. Energy* **2020**, *263*, doi:10.1016/j.apenergy.2020.114694.

Preprints.org (www.preprints.org) | NOT PEER-REVIEWED | Posted: 13 May 2024 doi:10.20944/preprints202405.0743.v1

6. Kelemen, P.; Benson, S.M.; Pilorgé, H.; Psarras, P.; Wilcox, J. An overview of the status and challenges of CO_2 storage in minerals and geological formations. *Front. Clim.* **2019**, *1*, doi:10.3389/fclim.2019.00009.
7. Sandalow, D.; Aines, R.; Friedmann, J.; Kelemen, P.; McCormick, C.; Power, I.M.; Schmidt, B.; Wilson, S.A.S. *Carbon Mineralization Roadmap*; 2021.
8. Seifritz, W. CO_2 disposal by means of silicates. *Nature* **1990**, *345*, 486-486, doi:10.1038/345486b0.
9. Gerdemann, S.J.; O'Connor, W.K.; Dahlin, D.C.; Penner, L.R.; Rush, H. Ex situ aqueous mineral carbonation. *Environ. Sci. Technol.* **2007**, *41*, 2587-2593, doi:10.1021/es0619253.
10. Power, I.M.; Harrison, A.L.; Dipple, G.M.; Wilson, S.; Kelemen, P.B.; Hitch, M.; Southam, G. Carbon mineralization: from natural analogues to engineered systems. *Rev. Mineral. Geochem.* **2013**, *77*, 305-360, doi:10.2138/rmg.2013.77.9.
11. Hills, C.D.; Tripathi, N.; Carey, P.J. Mineralization technology for carbon capture, utilization, and storage. *Front. Energy Res.* **2020**, *8*, doi:10.3389/fenrg.2020.00142.
12. Woodall, C.M.; McQueen, N.; Pilorgé, H.; Wilcox, J. Utilization of mineral carbonation products: current state and potential. *Greenh. Gases: Sci. Technol.* **2019**, *9*, 1096-1113, doi:10.1002/ghg.1940.
13. Zevenhoven, R.; Slotte, M.; Koivisto, E.; Erlund, R. Serpentinite carbonation process routes using ammonium sulfate and integration in industry. *Energy Technol.* **2017**, *5*, 945-954, doi:10.1002/ente.201600702.
14. Garcia, B.; Beaumont, V.; Perfetti, E.; Rouchon, V.; Blanchet, D.; Oger, P.; Dromart, G.; Huc, A.Y.; Haeseler, F. Experiments and geochemical modelling of CO_2 sequestration by olivine: Potential, quantification. *Appl. Geochem.* **2010**, *25*, 1383-1396, doi:10.1016/j.apgeochem.2010.06.009.
15. Oelkers, E.H.; Gislason, S.R.; Matter, J. Mineral carbonation of CO_2. *Elements* **2008**, *4*, 333-337, doi:10.2113/gselements.4.5.333.
16. Olajire, A.A. A review of mineral carbonation technology in sequestration of CO_2. *J. Petrol. Sci. Eng.* **2013**, *109*, 364-392, doi:10.1016/j.petrol.2013.03.013.
17. Sanna, A.; Uibu, M.; Caramanna, G.; Kuusik, R.; Maroto-Valer, M.M. A review of mineral carbonation technologies to sequester CO_2. *Chem. Soc. Rev.* **2014**, *43*, 8049-8080, doi:10.1039/c4cs00035h.
18. Zevenhoven, R.; Kavaliauskaite, I. Mineral carbonation for long-term CO_2 storage: an exergy analysis. *Int. J. Thermodyn.* **2004**, *7*, 23-31.
19. Hartmann, J.; West, A.J.; Renforth, P.; Köhler, P.; De La Rocha, C.L.; Wolf-Gladrow, D.A.; Dürr, H.H.; Scheffran, J. Enhanced chemical weathering as a geoengineering strategy to reduce atmospheric carbon dioxide, supply nutrients, and mitigate ocean acidification. *Rev. Geophys.* **2013**, *51*, 113-149, doi:10.1002/rog.20004.
20. Berner, R.A.; Lasaga, A.C.; Garrels, R.M. The carbonate-silicate geochemical cycle and its effect on atmospheric carbon dioxide over the past 100 million years. *Am. J. Sci.* **1983**, *283*, 641-683, doi:10.2475/ajs.283.7.641.
21. Raymo, M.E.; Ruddiman, W.F. Tectonic forcing of late Cenozoic climate. *Nature* **1992**, *359*, 117-122, doi:10.1038/359117a0.
22. Gaillardet, J.; Dupré, B.; Louvat, P.; Allègre, C.J. Global silicate weathering and CO_2 consumption rates deduced from the chemistry of large rivers. *Chem. Geol.* **1999**, *159*, 3-30, doi:10.1016/s0009-2541(99)00031-5.
23. Penman, D.E.; Caves Rugenstein, J.K.; Ibarra, D.E.; Winnick, M.J. Silicate weathering as a feedback and forcing in Earth's climate and carbon cycle. *Earth-Sci. Rev.* **2020**, *209*, doi:10.1016/j.earscirev.2020.103298.
24. Bearat, H.; McKelvy, M.J.; Chizmeshya, A.V.; Gormley, D.; Nunez, R.; Carpenter, R.W.; Squires, K.; Wolf, G.H. Carbon sequestration via aqueous olivine mineral carbonation: role of passivating layer formation. *Environ. Sci. Technol.* **2006**, *40*, 4802-4808, doi:10.1021/es0523340.
25. Gadikota, G.; Matter, J.; Kelemen, P.; Park, A.H. Chemical and morphological changes during olivine carbonation for CO_2 storage in the presence of NaCl and $NaHCO_3$. *Phys. Chem. Chem. Phys.* **2014**, *16*, 4679-4693, doi:10.1039/c3cp54903h.
26. Hariharan, S.; Mazzotti, M. Kinetics of flue gas CO_2 mineralization processes using partially dehydroxylated lizardite. *Chem. Eng. J.* **2017**, *324*, 397-413, doi:10.1016/j.cej.2017.05.040.
27. Kashim, M.Z.; Tsegab, H.; Rahmani, O.; Abu Bakar, Z.A.; Aminpour, S.M. Reaction mechanism of wollastonite in situ mineral carbonation for CO_2 sequestration: effects of saline conditions, temperature, and pressure. *ACS Omega* **2020**, *5*, 28942-28954, doi:10.1021/acsomega.0c02358.
28. Larachi, F.; Daldoul, I.; Beaudoin, G. Fixation of CO_2 by chrysotile in low-pressure dry and moist carbonation: Ex-situ and in-situ characterizations. *Geochim. Cosmochim. Acta.* **2010**, *74*, 3051-3075, doi:10.1016/j.gca.2010.03.007.
29. Li, W.; Li, W.; Li, B.; Bai, Z. Electrolysis and heat pretreatment methods to promote CO_2 sequestration by mineral carbonation. *Chem. Eng. Res. Design* **2009**, *87*, 210-215, doi:10.1016/j.cherd.2008.08.001.
30. Maroto-Valer, M.M.; Fauth, D.J.; Kuchta, M.E.; Zhang, Y.; Andrésen, J.M. Activation of magnesium rich minerals as carbonation feedstock materials for CO_2 sequestration. *Fuel Process. Technol.* **2005**, *86*, 1627-1645, doi:10.1016/j.fuproc.2005.01.017.

Preprints.org (www.preprints.org) | NOT PEER-REVIEWED | Posted: 13 May 2024 doi:10.20944/preprints202405.0743.v1

31. Styles, M.T.; Sanna, A.; Lacinska, A.M.; Naden, J.; Maroto-Valer, M. The variation in composition of ultramafic rocks and the effect on their suitability for carbon dioxide sequestration by mineralization following acid leaching. *Greenh. Gases: Sci. Technol.* **2014**, *4*, 440-451, doi:10.1002/ghg.1405.
32. Kwon, S. Mineralization for CO_2 sequestration using olivine sorbent in the presence of water vapor. Ph.D., Georgia Institute of Technology, Georgia, USA, 2011.
33. Kelemen, P.B.; Matter, J.; Streit, E.E.; Rudge, J.F.; Curry, W.B.; Blusztajn, J. Rates and mechanisms of mineral carbonation in peridotite: natural processes and recipes for enhanced, in situ CO_2 capture and storage. *Annu. Rev. Earth Planet. Sci.* **2011**, *39*, 545-576, doi:10.1146/annurev-earth-092010-152509.
34. Taylor, L.L.; Quirk, J.; Thorley, R.M.S.; Kharecha, P.A.; Hansen, J.; Ridgwell, A.; Lomas, M.R.; Banwart, S.A.; Beerling, D.J. Enhanced weathering strategies for stabilizing climate and averting ocean acidification. *Nat. Clim. Change* **2015**, *6*, 402-406, doi:10.1038/nclimate2882.
35. Brady, P.V. The effect of silicate weathering on global temperature and atmospheric CO_2. *J. Geophys. Res. Solid Earth* **2012**, *96*, 18101-18106, doi:10.1029/91jb01898.
36. Power, I.M.; Paulo, C.; Rausis, K. The mining industry's role in enhanced weathering and mineralization for CO_2 removal. *Environ. Sci. Technol.* **2024**, *58*, 43-53, doi:10.1021/acs.est.3c05081.
37. Edwards, D.P.; Lim, F.; James, R.H.; Pearce, C.R.; Scholes, J.; Freckleton, R.P.; Beerling, D.J. Climate change mitigation: potential benefits and pitfalls of enhanced rock weathering in tropical agriculture. *Biol. Lett.* **2017**, *13*, 1-7, doi:10.1098/rsbl.2016.0715.
38. Haque, F.; Santos, R.M.; Chiang, Y.W. CO_2 sequestration by wollastonite-amended agricultural soils – an Ontario field study. *Int. J. Greenh. Gas Control* **2020**, *97*, doi:10.1016/j.ijggc.2020.103017.
39. Moosdorf, N.; Renforth, P.; Hartmann, J. Carbon dioxide efficiency of terrestrial enhanced weathering. *Environ. Sci. Technol.* **2014**, *48*, 4809-4816, doi:10.1021/es4052022.
40. Power, I.M.; Dipple, G.M.; Bradshaw, P.M.D.; Harrison, A.L. Prospects for CO_2 mineralization and enhanced weathering of ultramafic mine tailings from the Baptiste nickel deposit in British Columbia, Canada. *Int. J. Greenh. Gas Control.* **2020**, *94*, doi:10.1016/j.ijggc.2019.102895.
41. Strefler, J.; Amann, T.; Bauer, N.; Kriegler, E.; Hartmann, J. Potential and costs of carbon dioxide removal by enhanced weathering of rocks. *Environ. Res. Lett.* **2018**, *13*, doi:10.1088/1748-9326/aaa9c4.
42. Falk, E.S.; Kelemen, P.B. Geochemistry and petrology of listvenite in the Samail ophiolite, Sultanate of Oman: Complete carbonation of peridotite during ophiolite emplacement. *Geochim. Cosmochim. Acta.* **2015**, *160*, 70-90, doi:10.1016/j.gca.2015.03.014.
43. Kelemen, P.B.; Hirth, G. Reaction-driven cracking during retrograde metamorphism: olivine hydration and carbonation. *Earth Planet. Sci. Lett.* **2012**, *345-348*, 81-89, doi:10.1016/j.epsl.2012.06.018.
44. Goff, F.; Lackner, K.S. Carbon dioxide sequestering using ultramafic rocks. *Environ. Geosci.* **1998**, *5*, 89-102, doi:10.1046/j.1526-0984.1998.08014.x.
45. Mervine, E.M.; Humphris, S.E.; Sims, K.W.W.; Kelemen, P.B.; Jenkins, W.J. Carbonation rates of peridotite in the Samail Ophiolite, Sultanate of Oman, constrained through 14C dating and stable isotopes. *Geochim. Cosmochim. Acta.* **2014**, *126*, 371-397, doi:10.1016/j.gca.2013.11.007.
46. Streit, E.; Kelemen, P.; Eiler, J. Coexisting serpentine and quartz from carbonate-bearing serpentinized peridotite in the Samail Ophiolite, Oman. *Contribut. Mineral. Petrol.* **2012**, *164*, 821-837, doi:10.1007/s00410-012-0775-z.
47. Cutts, J.A.; Steinthorsdottir, K.; Turvey, C.; Dipple, G.M.; Enkin, R.J.; Peacock, S.M. Deducing mineralogy of serpentinized and carbonated ultramafic rocks using physical properties with implications for carbon sequestration and subduction zone dynamics. *Geochem. Geophys. Geosystems.* **2021**, *22*, doi:10.1029/2021gc009989.
48. Lisabeth, H.P.; Zhu, W.; Kelemen, P.B.; Ilgen, A. Experimental evidence for chemo-mechanical coupling during carbon mineralization in ultramafic rocks. *Earth Planet. Sci. Lett.* **2017**, *474*, 355-367, doi:10.1016/j.epsl.2017.06.045.
49. Paulo, C.; Power, I.M.; Zeyen, N.; Wang, B.; Wilson, S. Geochemical modeling of CO_2 sequestration in ultramafic mine wastes from Australia, Canada, and South Africa: implications for carbon accounting and monitoring. *Appl. Geochem.* **2023**, *152*, doi:10.1016/j.apgeochem.2023.105630.
50. DMR. *Geology of Thailand*, 1st ed.; Department of Mineral Resources, Ministry of Natural Resources and Environment: Bangkok, Thailand, 2014.
51. Phajuy, B.; Panjasawatwong, Y.; Osataporn, P. Preliminary geochemical study of volcanic rocks in the Pang Mayao area, Phrao, Chiang Mai, northern Thailand: tectonic setting of formation. *J. Asian Earth Sci.* **2005**, *24*, 765-776, doi:10.1016/j.jseaes.2004.06.001.
52. Barr, S.M.; Tantisukrit, C.; Yaowanoiyothin, W.; Macdonald, A.S. Petrology and tectonic implications of Upper Paleozoic volcanic rocks of the Chiang Mai belt, northern Thailand. *J. Southeast Asian Earth Sci.* **1990**, *4*, 37-47, doi:10.1016/0743-9547(90)90023-7.
53. Metcalfe, I. Permian tectonic framework and palaeogeography of SE Asia. *J. Asian Earth Sci.* **2002**, *20*, 551-566, doi:10.1016/s1367-9120(02)00022-6.
54. DMR. Geological map of Thailand on 1:50,000 scale. **2007**.

Preprints.org (www.preprints.org) | NOT PEER-REVIEWED | Posted: 13 May 2024 doi:10.20944/preprints202405.0743.v1

55. Le Maitre, R.W.; Streckeisen, A.; Zanettin, B.; Le Bas, M.J.; Bonin, B.; Bateman, P., (Eds.) *Igneous rocks: a classification and glossary of terms: recommendations of the international union of geological sciences subcommission on the systematics of igneous rocks*. 2 ed.; Cambridge University Press: Cambridge, England, 2002.
56. Feniak, M.W. Grain sizes and shapes of various minerals in igneous rocks. *American Mineralogist* **1944**, *29*, 415–421.
57. Liu, L.; Liu, Y.; Tian, X.; Chen, X. Superior CO_2 uptake and enhanced compressive strength for carbonation curing of cement-based materials via flue gas. *Constr. Build. Mater.* **2022**, *346*, doi:10.1016/j.conbuildmat.2022.128364.
58. Nielsen, P.; Quaghebeur, M. Determination of the CO_2 uptake of construction products manufactured by mineral carbonation. *Minerals* **2023**, *13*, doi:10.3390/min13081079.
59. Yang, K.-H.; Seo, E.-A.; Tae, S.-H. Carbonation and CO_2 uptake of concrete. *Environ. Impact Assess. Rev.* **2014**, *46*, 43-52, doi:10.1016/j.eiar.2014.01.004.
60. Raza, A.; Glatz, G.; Gholami, R.; Mahmoud, M.; Alafnan, S. Carbon mineralization and geological storage of CO_2 in basalt: mechanisms and technical challenges. *Earth-Sci. Rev.* **2022**, *229*, doi:10.1016/j.earscirev.2022.104036.

Disclaimer/Publisher's Note: The statements, opinions and data contained in all publications are solely those of the individual author(s) and contributor(s) and not of MDPI and/or the editor(s). MDPI and/or the editor(s) disclaim responsibility for any injury to people or property resulting from any ideas, methods, instructions or products referred to in the content.